A Paper-Based All-in-One Origami Nanobiosensor for Point-of-Care Detection of Cardiac Protein Markers in Whole Blood

Hao Fu,[1,2,3,‡] Zhen Qin,[1,‡] Xiao Li,[2] Yueyue Pan,[1] Haitong Xu,[1] Peng Pan,[1] Pengfei Song,[4] and Xinyu Liu[1,5]*

[1] Department of Mechanical and Industrial Engineering, University of Toronto, ON M5S 3G8, Canada

[2] Department of Mechanical Engineering, McGill University, Montreal, QC H3A 0C3, Canada

[3] Shenzhen Mindray Bio-Medical Electronics Co., Ltd., Shenzhen, Guangdong 518058, China

[4] School of Advanced Technology, Xi'an Jiaotong-Liverpool University, Suzhou, Jiangsu 215123, China

[5] Institute of Biomedical Engineering, University of Toronto, ON M5S 3G9, Canada

‡ These authors contributed equally to this work.

* Corresponding author: +1-416-946-0558; xyliu@mie.utoronto.ca

ABSTRACT

Rapid and accurate diagnosis of cardiovascular diseases (CVDs) at the earliest stage is of paramount importance to improve the treatment outcomes and avoid irreversible damage to a patient's cardiovascular system. Microfluidic paper-based devices (μPADs) represent a promising platform for rapid CVD protein biomarker diagnosis at the point of care (POC). This paper presents an electrochemical μPAD (E-μPAD) with an all-in-one origami design for rapid and POC testing of cardiac protein markers. Based on the label-free, electrochemical impedance spectroscopy (EIS) immunoassay, the E-μPAD integrates all essential components on a single chip, including three electrochemical cells, a plasma separation membrane, and a buffer absorption pad, enabling easy and streamlined operations for multiplexed detection of three cardiac protein markers [cardiac troponin I (cTnI), brain natriuretic peptide (BNP)-32, D-Dimer] on a finger-prick whole blood sample within 46 minutes. Superior analytical performance is achieved through sensitive EIS

measurement on carbon electrodes decorated with semiconductor zinc oxide nanowires (ZnO NWs). Using spiked human plasma samples, ultralow limits of detection (LODs) of the E-µPAD are achieved at 4.6 pg/mL (190 fM) for cTnI, 1.2 pg/mL (40 fM) for BNP-32, and 146 pg/mL (730 fM) for D-Dimer. Real human blood samples spiked with purified proteins are also tested, and the device's analytical performance was proven comparable to commercial ELISA kits. The all-in-one E-µPAD will allow rapid and sensitive testing of cardiac protein markers through easy operations, which holds great potential for on-site screening of acute CVDs in non-laboratory settings such as emergency rooms, doctor's offices, or patient homes.

Keywords: Cardiovascular disease; Cardiac biomarker; Electrochemical impedance spectroscopy; Paper-based microfluidics; Zinc oxide nanowire

Cardiovascular diseases (CVDs) are the leading cause of death worldwide, and approximately 17.9 million people died from CVDs in 2019, representing 32% of the worldwide deaths [1]. Due to the irreversible damages to the cardiovascular system caused by CVDs, accurate and rapid CVD diagnosis at the earliest stage is of paramount importance for improving the treatment outcomes and saving patients' lives. An internationally recognized guideline recommends a turnaround time of CVD testing within 60 minutes to enable timely treatments for patients who may suffer from CVDs [2]. However, less than 25% of the global hospitals can meet the recommended turnaround time requirement [3]. To identify the specific type of CVD such as acute coronary syndrome (ACS) or heart failure, immunoassays such as enzyme-linked immunosorbent assay (ELISA) and lateral flow immunoassay (LFIA) have been used as the gold standard tests for detecting specific cardiac biomarkers; in particular, the LFIA has been widely adopted in hospital emergency rooms because of its short assay time (<15 min). However, typical LFIAs provide limited sensitivity for the detection of early-stage CVDs. The further development of rapid CVD diagnostic tools with high clinical performance can help shorten the delay in CVD diagnosis and thus lead to promote treatment outcomes [4].

Rapid on-site diagnosis of infectious diseases has become increasingly important, which was recently highlighted by the ongoing COVID-19 pandemic [5]. Significant efforts have been devoted to developing microfluidic platforms for point-of-care (POC) blood testing of cardiac biomarkers [6–9], which are typically constructed from elastomer (e.g., polydimethylsiloxane – PDMS) and plastic materials and employ a variety of biosensing mechanisms including electrochemistry [4,10–12] and chemiluminescence [13–18]. In addition, several microfluidic diagnostic devices are commercially available for Cardiac Troponin I (cTnI) and Cardiac Troponin T (cTnT) detection [19], such as the i-STAT System from Abbott [20] and the Triage Meter Pro from Quidel [21].

Besides the conventional PDMS- and plastic-based microfluidic devices, microfluidic paper-based analytical devices (µPADs) represent another promising platform technology for CVD diagnostics. The µPADs offer a unique combination of advantages such as pumpless fluid transport, simple device fabrication, mature analytical chemistry on paper substrates, low material and manufacturing costs, and high portability [7,22–24]. In addition, µPADs with novel three-dimensional origami designs allow for high-level device integration and simple operations, which are particularly suitable for use in non-laboratory environments by un-skilled users [25–27]. Detection of protein biomarkers based on electrochemical mechanisms has been widely performed on µPADs with screen-printed electrodes [28,29] providing higher sensitivities than colorimetric methods. With the addition of functional nanomaterials such as carbon nanotubes [30] and graphene [31,32] on working electrodes (WEs), these electrochemical µPADs (E-µPADs) are capable of detecting low-concentration protein analytes with ultra-high sensitivities.

Compared to these carbon-based nanomaterials that are normally synthesized off the chip, semiconductor zinc oxide nanowires (ZnO NWs) can be directly grown on a paper electrode through a low-temperature hydrothermal process [33–36]. The *in-situ* decoration of an E-µPAD electrode with ZnO NWs greatly improves the electrode's surface-area-to-volume ratio and thus the device's analytical sensitivity. Only a few reports have focused on developing E-µPADs for POC detection of cardiac protein markers [37–40]. These studies are mainly about multiplexing device designs for the detection of multiple cardiac markers [37], WE decoration methods with different nanomaterials and protein capture probes [38,39], and assay optimization experiments for improving the analytical performance [37]. However, there is no integrated device design with all required components on the same chip (an "all-in-one" design) for rapid and sensitive CVD diagnosis. Electrochemical impedance spectroscopy (EIS) is a powerful technique to rapidly analyse the bio-

recognition events occurring at the electrode surface [41,42]. The proven biosensing technique requires no molecule labelling for signal readout and directly measures the impedance spectroscopy of the WE-solution interface as a function of the target analyte amount captured on the WE surface [34,43]. The EIS-based biosensing provides high sensitivity, satisfactory selectivity, simple assay operation and short turnaround time.

This paper reports an all-in-one origami E-µPAD for multiplexed detection of three major cardiac protein markers, namely cTnI, brain natriuretic peptide (BNP)-32, and D-Dimer. The detection of cardiac protein markers helps clinicians further enhance myocardial infarction (MI) rule out with results obtained by an on-site clinical specialist. The measurement of a specific marker also reveals the condition's specificity, myocardial damage location, and the initial time of on-set/progression. However, no single cardiac protein biomarker can be considered as a general indicator for all possible conditions due to the complexity of CVDs. Therefore, the rapid test of multiple cardiac biomarkers within desired turnaround time is significant for assessing patients with potential CVDs [7]. Among the biomarkers, cTnI or cTnT has the highest cardio-specificity. It is elevated within a few hours of heart damage and remains elevated for up to two weeks. The rising levels in a series of troponin tests performed over several hours can help diagnose a heart attack [44,45]. BNP-32 is used to recognize heart failure, and its increased level in patients with ACS indicates an increased risk of recurrent events [46]. D-Dimer is the marker with high sensitivity and relatively high specificity for differentiating MI from unstable angina (UA) in patients with suspected ACS [47]. The proposed integrated origami E-µPAD includes three electrochemical biosensors (for multiplexed cardiac marker detection), a plasma separation membrane (for whole blood processing into plasma), and an absorption pad (for electrode washing and absorption). Based on label-free electrochemical impedance spectroscopy (EIS) detection that monitors the

impedance (ratio between current and voltage) or capacitance changes at the electrode interface, this device is capable of rapidly testing a whole blood sample within 46 min through a few operation steps starting from a finger prick. The WE of each electrochemical biosensor is coated with semiconductor ZnO NWs to increase the surface-area-to-volume ratio of the WE and thus achieve a high sensitivity of the EIS detection. The analytical performance of the E-μPAD is characterized using both artificial plasma samples and whole blood samples spiked with the three cardiac markers, and the picogram/mL-level limits of detection (LODs) are achieved.

EXPERIMENTAL SECTION

Design of the all-in-one origami E-μPAD. The all-in-one origami E-μPAD (Fig. 1) consists of four functional paper areas (connected by laser-cut folding hinges), including: (i) a central sensing area with three ZnO-NW-coated carbon WEs, (ii) a left plasma separation flap, (iii) a right buffer absorption flap, and (iv) a top signal readout flap. The three paper flaps can be readily folded onto the central sensing area, thus allowing easy fluid manipulation and a signal readout on the three WEs. The top signal readout flap includes three wax-patterned paper test zones (diameter: 6 mm), and each of the test zones has a carbon counter electrode (CE) and a silver/silver chloride (Ag/AgCl) reference electrode (RE) patterned on its back surface (Figs. 1a and 1b). Once folded onto the central biosensing area, these test zones on the signal readout flap will have intimate contact with the three WEs, thus forming three electrochemical cells for EIS-based protein detection. The detailed fabrication process and materials involved for the E-μPAD are described in the following section.

The WE was fabricated from a piece of laser-cut cellulose paper (Fig. 1b), which was first screen-printed with carbon ink (as the sensing area) and Ag/AgCl ink (as an electrical connection) and then decorated with ZnO NWs (in its circular sensing area). The detailed fabrication process

of the WE is described in Supplementary Note 1. The prepared WE was then assembled onto the paper chip central sensing area with a piece of double-sided tape. A piece of cookie paper, laser-cut into complementary shapes of the three WEs, was used to cover the remaining area of the double-sided tape to avoid undesired adhesion during device operation (Fig. 1a). The left plasma separation flap was patterned into three hydrophilic paper zones (with the same diameter as the WEs) well aligned with the positions of the three WEs in the central sensing area. A commercial circular plasma separation membrane was attached to the back surface of the left flap through plastic lamination, which serves as the sample inlet of the E-µPAD. The integrated membrane filters the added whole blood sample to allow only the plasma passing through the three circular paper zones and reach the individual WEs. The right absorption flap was attached with a piece of 16 mm × 16 mm chromatography cellulose paper as a thick absorption pad (Whatman CHR 3MM, GE Healthcare), which can be folded onto the central area to absorb buffer solution off the WEs during the washing step. Fig. 1c presents the photographs of the fabricated E-µPAD.

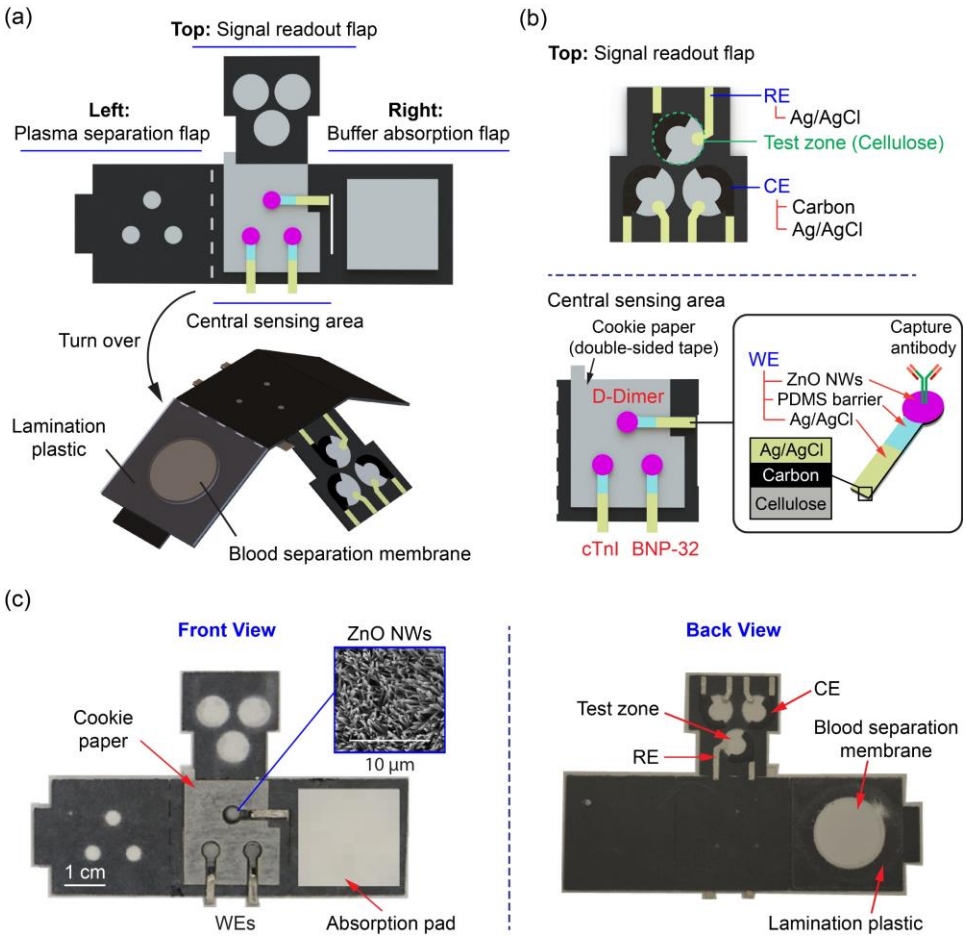

Figure 1. *Schematic illustration of the origami all-in-one E-μPAD. (a) The three-dimensional schematics of the E-μPAD. (b) The schematic design of the electrodes in the three electrochemical cells of the E-μPAD (WE: working electrode, RE: reference electrode, and CE: counter electrode). (c) Photographs of the fabricated E-μPAD.*

Fabrication of the E-μPAD and ZnO NWs integrated WEs. To describe the E-μPAD fabrication process in detail, a piece of chromatography cellulose paper (cat. #Whatman CHR #1, GE Healthcare) was firstly patterned by wax printing using a commercial wax printer (cat. #ColorQube 8570, Xerox) to define the hydrophilic paper zones on the signal readout flank and the plasma separation flank (Fig. 1a). The printed paper was then baked on a hot plate at 130 °C for 2 minutes to allow the printed wax to melt and penetrate the cellulose paper matrix, thus

forming the hydrophobic wax barriers and the confined hydrophilic paper zones (Fig. 1a). The wax patterned paper was then laser-cut into pre-designed shapes with a CO_2 laser cutter (VLS 2.30, Universal Laser Systems), and the fold lines between flanks were laser-cut with dashed line settings for easy folding. Carbon ink (cat. #E3456, Ercon) was screen-printed on the three test zones on the top signal readout flap and then baked on one hotplate at 65 °C for 20 minutes to dry and form three carbon CEs. Similarly, Ag/AgCl ink was screen-printed on the same flap as three REs, meanwhile it was also printed on the carbon CEs as the electrical contact strips. The printing of Ag/AgCl ink also followed the drying at 65 ℃ for 20 minutes.

To fabricate the WEs, a piece of chromatography cellulose paper (cat. #Whatman CHR #1, GE Healthcare) was laser-cut into arrays of four pristine paper WEs with their non-circular ends connected by a paper strip. One side of the paper WE array was then screen-printed with carbon ink and dried on 65 °C for 20 minutes. To further confine the solution within the circular WE region for a stable assay performance, polydimethylsiloxane (PDMS) mixing with a base: curing agent ratio of 10:1 was brushed onto the neck region of a WE strip to form hydrophobic barriers (Fig. 1b). An extra layer of Ag/AgCl was also printed on the tail of the carbon WE to enhance the electrical conductivity. The circular area of the carbon WE was coated with ZnO NWs through the low-temperature hydrothermal growth method (described in Supplementary Note 1) and afterwards functionalized with the CVD capture antibodies. The WEs were fabricated in batches through the process, thus enabling mass-scale production. The prepared WE with ZnO NWs was attached to the central area of the origami paper chip with a piece of double-sided adhesive tape (cat. #Cont. 1 Roll, 3M) (Fig. 1b).

Following the construction of the three electrochemical cells, other device components were assembled, such as a circular plasma separation membrane on the left flap and a paper absorption

pad on the right flap. The commercial plasma separation membrane (Vivid Plasma Separation Membrane, Pall Life Sciences) was laser-cut into a circular disk with a diameter of 6.5 mm and then attached to the backside of the left plasma separation flap using a single-sided plastic tape (L&B cold laminating film, Quaff) through lamination (TL902-C laminator machine, Scotch). One piece of thick chromatography cellulose paper (cat. #Whatman CHR 3MM, GE Healthcare) with a dimension of 16 mm × 16 mm was used as the absorption pad and attached to the right flap with a piece of double-sided adhesive tape (Fig. 1c).

Biofunctionalization of the ZnO NWs integrated WEs. Following the growth of ZnO NWs on the carbon WE, the saline-based surface chemical modification process was performed on the NWs to increase the active site number for the covalent binding of capture antibodies [34]. An air plasma gun (Corana SB, BlackHole Lab) was used to treat oxygen plasma on the ZnO-NW surface to generate hydroxyl (-OH) groups. Afterwards two arrays of plasma treated WEs were immersed into a glass vial with 25 mL of 10 mM (3-aminopropyl)trimethoxysilane in ethanol (APTMS; cat. #281778, Sigma-Aldrich). The glass vial was then sealed and heated in an oven at 80 ℃ for 2 hours. The WEs were then washed with ethanol and dried on one hotplate at 80 ℃ for 10 minutes to remove excessive APTMS on the ZnO NWs. Next 3 μL of 2.5% v/v in glutaraldehyde (GA, cat. #G7776 from Sigma-Aldrich) in DI water was added to the WEs for a 30-minute incubation at room temperature, which was repeated twice. Finally, extra GA on the WEs was washed away with DI water, followed by drying on the hotplate of 80 ℃ for 10 minutes.

The capture antibody solutions of 10 μg/mL anti-cTnI (cat. #ab47003, Abcam), 10 μg/mL anti-BNP-32 (cat. #sc-271185, Santa Cruz Biotechnology), and 40 μg/mL anti-D-Dimer (cat. #ab10050, Abcam) were prepared from their stock solutions. Then, 3 μL of each capture antibody solution was pipetted onto the circular area of a ZnO-NW-coated WE. The antibody-coated WEs were

incubated in a refrigerator at 4 °C for 2 hours. 8 μL of washing buffer [1× phosphate buffered saline (PBS) with 0.05% (v/v) Tween 20; cat. #P4417 and P1379 from Sigma-Aldrich, respectively] was added to each WE and then blotted by the absorption paper to wash away the unbound capture antibodies. Next, 3 μL of a commercial blocking reagent (cat. #11152500, Roche) was pipetted to each WE and dried at room temperature for 30 minutes. Finally, each WE was washed with 8 μL of washing buffer and dried at room temperature to be ready for device assembly.

Operation of the origami E-μPAD. The developed E-μPAD can detect the three cardiac protein markers simultaneously on a single device. The simple operation steps are illustrated in Fig. 2. Firstly, the left plasma separation flap was folded onto the central sensing area with its edge inserted into the laser-cut slot at the folding hinge of the right buffer absorption flap to ensure an intimate contact of the three paper zones of the left flap with the WEs. Then, 20 μL of whole blood sample from a finger prick was added to the sample inlet of the plasma separation membrane (Fig. 2a). It generally took 20 minutes for the blood sample to pass the membrane and reach the three WEs (Fig. 2b). Approximately 3 μL of human plasma reached each WE, which fit the experimentally confirmed wicking capacity of the circular WE area and the typical 45% v/v ratio of plasma in the whole blood. After the plasma separation step, the left flap was torn off at its folding hinge. 8 μL of washing buffer was then pipetted onto each WE to wash off unbound proteins, and the right absorption flap was folded onto the central sensing area to blot the excessive washing buffer from the three WEs (Fig. 2c). The washing step reduced the non-specific binding on the WE and thus decreased the background noise of the EIS measurement. The right flap was followingly removed and the cookie paper that covers the beneath double-sided tape was revealed (Fig. 2d). The top signal readout flap was folded onto the central area for EIS measurement (Fig. 2e). 4 μL of electron mediator solution [5 mM $K_3[Fe(CN)_6]$/$K_4[Fe(CN)_6]$ (cat. #244023/P3289,

Sigma-Aldrich) in 100 mM KCl solution (cat. #44675, Sigma-Aldrich)] was added to the test zone, and the three WEs of the biosensor were connected to a precise potentiostat (Autolab PGSTAT302N, Metrohm) for performing EIS measurement (Fig. 2f). The software NOVA Autolab (version 2.1.4, Metrohm) was used for the electrochemical circle fit to find the corresponding electron transfer resistance R_{et} values of the WE-solution interface. The fitting of the model to the experimental data was performed using complex nonlinear least-squares procedures available in the EIS data fitting function in the software. The entire assay on the E-μPAD for the simultaneous detection of the three CVD biomarkers typically takes around 46 minutes.

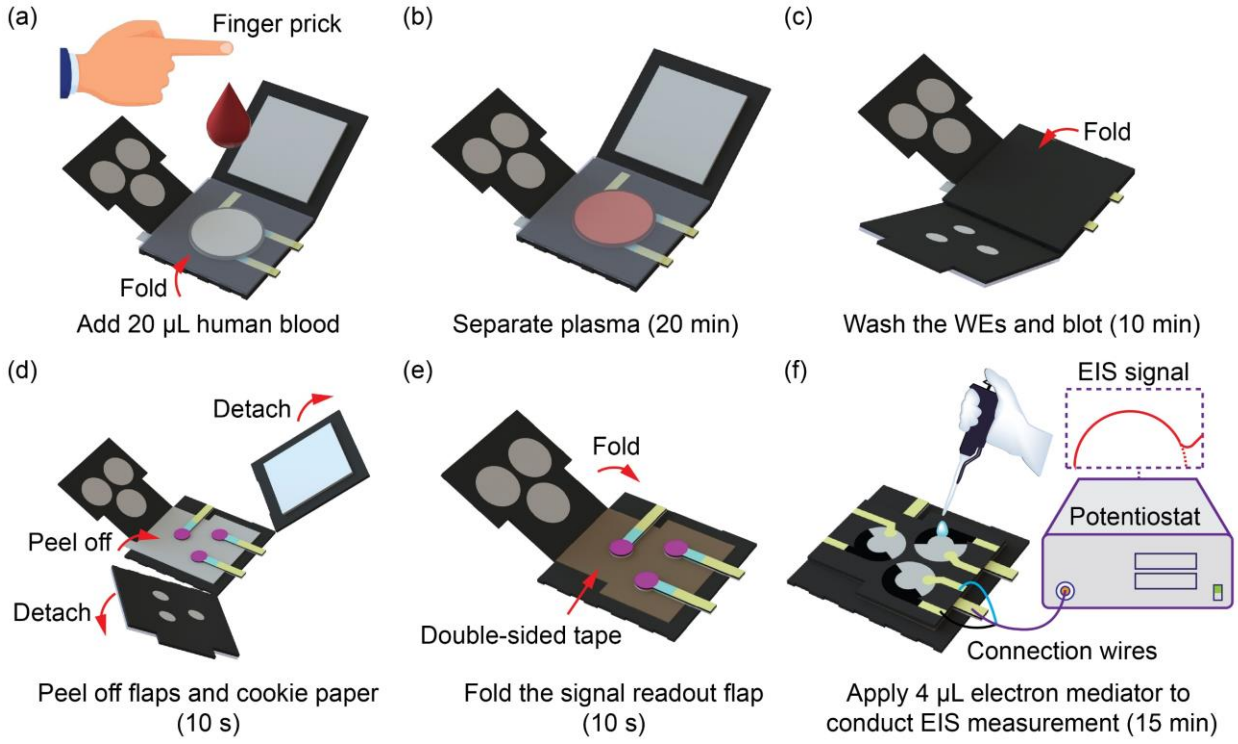

Figure 2. *The operation procedure of the E-μPAD for multiplexed detection of the three cardiac protein markers in whole blood from a finger prick, including (a) the addition of 20 μL of human blood sample, (b) incubation for 20 min to allow the plasma separation, (c) washing of the WEs with washing buffer and blotting the excessive reagents by folding the right buffer absorption flap (10 min), (d) peeling off the flaps*

and cookie paper (10 s), (e) folding the signal readout flap (10 s) and (f) application of 4 μL of electron mediator to conduct EIS measurement (15 min).

RESULTS AND DISCUSSION

EIS characterization of the E-μPAD. The surface morphologies of the ZnO NWs integrated WEs were observed and investigated with scanning electron microscopy (SEM) imaging (model: JEOL JSM6610-Lv) in comparison with the pristine cellulose paper chip and the carbon-printed WEs (Figs. S1a-c). Uniform porous structures with an estimated pore size of around 11 μm were observed on the pristine cellulose paper (Fig. S1a). A less porous surface was observed after carbon printing and the carbon layer was measured to be 30 μm (Fig. S1b). The ZnO NWs grew on the carbon surface successfully and presented a highly uniform distribution (Fig. S1c). Based on image analysis in ImageJ software, the average width and length of the synthesized ZnO NWs were measured to be ~291.5 ± 58.3 nm and 4.4 ± 0.88 μm respectively (n=5). The ZnO NW density was estimated to be ~4.6 nanowires/μm^2.

The developed origami E-μPAD employs the EIS sensing mechanism, which features label-free protein marker detection and an ultrasensitive performance [34,43]. EIS measures the interface impedance of the WE and the solution as a function of the amount of target protein captured on the WE surface. $K_3[Fe(CN)_6]/K_4[Fe(CN)_6]$ was selected as the electron mediator to provide the $Fe(CN)_6^{3+/4+}$ pair for the formation of a Faradic current [48,49]. The widely adopted equivalent circuit model [50] was used to describe the electron-transferring process during EIS measurement and extract the impedance of the WE-solution interface (Fig. 3a). The involved variables R_s, Z_w, R_{et} and C_{dl} represent the resistance of the solution, the Warburg impedance of diffusion in the proximity of the WE surface, the electron transfer resistance of the WE-solution interface, and the double layer capacitance on the WE surface respectively. R_{et} represents the insulation level of the

WE surface, and is inversely proportional to the standard rate constant of the electrochemical reaction, and the concentration of the redox probe components. The Warburg impedance Z_w quantifies the effect of diffusion on the total impedance, and depends on the diffusion coefficients of the redox couple. As diffusion and electron transfer are successive process, R_{et} and Z_w are coupled in series to form the faradaic impedance Z_F. Z_w is typically negligible at high frequencies, thus the "dome" regions in the Nyquist plots are generated by R_{et} and C_{dl} in parallel. When the target protein binds on the WE surface, the electron transfer efficiency at the electrode-solution interface decreased and the corresponding R_{et} value as the label-free EIS readout increases (Fig. 3a). It equals the diameter of the "dome" shape of the Nyquist plot, extracted from the model fitting with the potentiostat software [34]. The R_{et} was used to establish the response curve with the target concentration [41]. Fig. 3b presented two schematic Nyquist plots before and after the antigen was recognized by the capture probe on the ZnO NWs. The semicircular dome region expands after the recognition of the target protein on the WE surface, corresponding to an increase in the R_{et} value in the equivalent circuit model with the R_s remaining constant.

To characterize the electrochemical performance of the all-in-one origami E-μPAD, cyclic voltammetry (CV) was used to confirm the equilibrium potential of the redox pair, $[Fe(CN)_6]^{3-}/[Fe(CN)_6]^{4-}$, in the electron mediator solution. 3 μL of rabbit immunoglobulin G (IgG) (at 1 ng/mL; cat. #I5006, Sigma-Aldrich) and 3 μL of rabbit IgG antibody (at 25 μg/mL; cat. #R5506, Sigma-Aldrich) was used as the model target antigen and capture probe. The CV testing applied a linear sweeping voltage from −0.5V to 0.5V. Fig. 3c shows the measured cyclic voltammograms of the ZnO-NW-coated WEs before and after the target protein conjugation in comparison with the carbon-printed WEs. The CV current measured from the ZnO-NW-coated WE decreased after the capture probe immobilization. With the rabbit IgG captured on the WE

surface, the electron transfer rate on the WE became lower, and thus the CV current response was further reduced. The CV peak potential of the ZnO-NW-coated WE was found to be 5.5 times higher than that of the pristine carbon WE, which is attributed to the superior electron-transfer property and the enhanced surface-area-to-volume ratio [51]. The CV curves shared the same equilibrium potential at 245 mV under the different WE surface conditions. The value matched well with the one in the previous study, representing good repeatability for ZnO-NW decoration on E-µPAD [34]. It was applied as the direct current (DC) offset in the following EIS measurements.

The EIS output change with the binding of the rabbit IgG and the anti-rabbit IgG immobilized on the E-µPAD WEs were also compared at different surface conditions. A 5-mV alternating current (AC) voltage with a frequency varying from 20 kHz to 20 Hz was applied for the EIS measurement. Fig. 3d shows the measured Nyquist plots. In the high frequency (semi-circular dome region), Z_w was negligible and C_{dl} and R_{et} were thus in parallel connection. The R_s values under two conditions (the WE with and without target antigen) were confirmed to be almost the same, and the diameter of the dome shape indicates the R_{et} value. The EIS measurement confirmed that the R_{et} value increased after the recognition of the target antigen by the capture probe on the WE surface. The frequency range of 20 kHz-20 Hz was applied in the following EIS measurement as well.

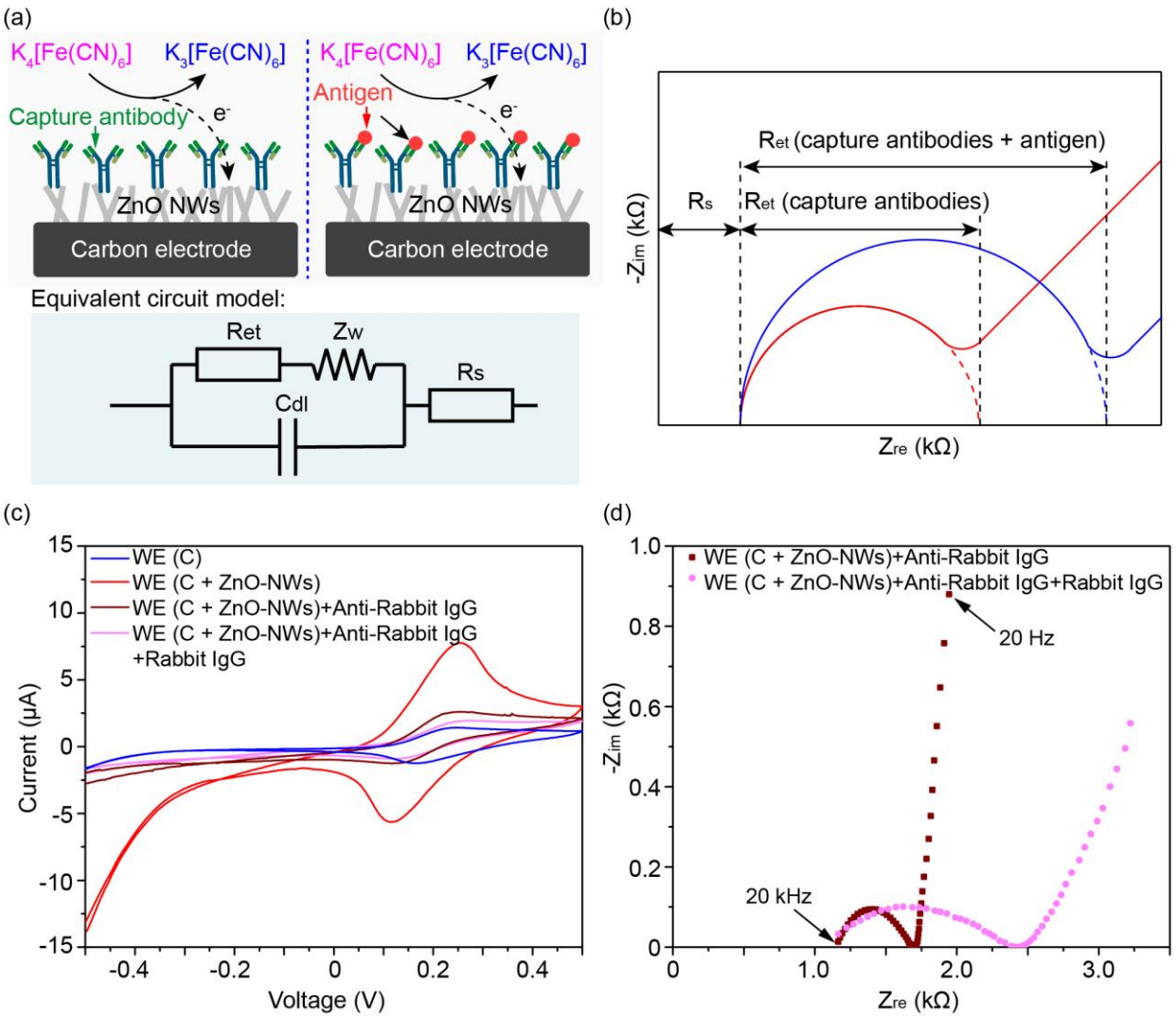

Figure 3. *The sensing mechanism of label-free EIS-based immunoassay on the E-μPAD. (a) Schematic diagrams (top) and the equivalent circuit model (bottom) of the charge transport process at the WE-solution interface. (b) Schematic illustration of two typical Nyquist plots reflecting the different surface coating conditions on the ZnO NWs before and after target antigen was recognized. (c) Experimental data of cyclic voltammograms measured under four different WE surface conditions. (d) Experimental data of two Nyquist plots measured from two WEs, one only coated with anti-rabbit-IgG capture probes (3 μL, 25 μg/mL) and the other coated with the capture probes and then recognized rabbit IgG antigen (3 μL, 1 ng/mL) (EIS frequency range: 20 Hz - 20 kHz).*

Integration and testing of the plasma separation membrane. The integration of a plasma separation membrane on the E-μPAD was studied to achieve an improved efficiency of plasma filtration and minimized leakage of the non-plasma compositions from the whole blood sample. The Vivid™ Plasma Separation Membrane (GX grade, Pall Life Sciences) that is effective for plasma separation on μPADs was applied [52–54]. Five circular plasma separation membranes with different diameters (10 mm, 11 mm, 12 mm, 13 mm, and 14 mm) were integrated onto the wax-printed left flap of the E-μPAD through lamination for testing the separation performance. Mimic E-μPADs with only the membrane integrated left flap and dummy WEs on the central sensing flap were fabricated (Fig. 4a). 3 μL of bromocresol green (BCG) solution (concentration: 0.04 wt% in DI water; cat. #114359, Millipore Sigma) was added to each dummy WE as the indicator to visualize the filtered plasma onto the dummy WEs [55], which showed light yellow color on paper initially as the baseline. 20 μL of commercial human blood (BioreclamationIVT, LLC, cat. #HUMANWBK2-0000409) was added to the inlet of the membrane for filtration of 20 minutes before visual inspection of the colour change. The change from the yellow to teal colour on the BCG zone indicated a successful plasma separation. Figs. 4b-4d illustrate the colorimetric readouts with different diameters of the plasma separation membranes. With a small blood separation membrane, the 20 μL of blood sample exceeded the membrane retention capacity for the non-plasma components, and the blood leaked onto the dummy WEs underneath, forming a brown mixture on the BCG zone (Fig. 4b). In contrast, an oversized blood separation membrane caused insufficient osmotic pressure for plasma penetration and delivery onto the dummy WEs (Fig. 4d). The plasma separation is regarded as successful only when a dummy WE turned into a teal colour (Fig. 4c). The counted success rates for different blood separation membranes were summarized

in Table 1 (n=21 dummy WEs for each membrane diameter). The one with a 13 mm diameter showed the highest success rate of 95.2% and was selected for the E-μPAD.

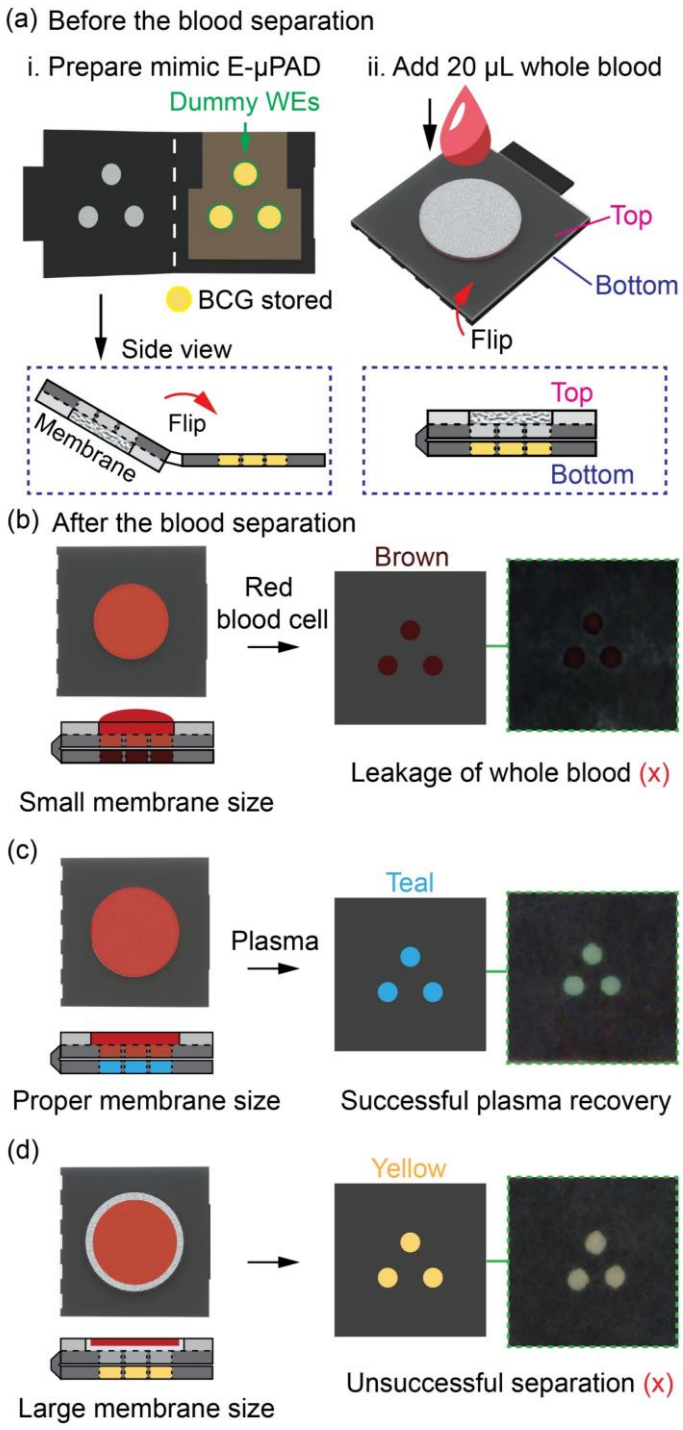

Figure 4. *Testing of different sizes of membranes for plasma separation. (a) Schematics of the testing mimic E-μPAD and mechanism. (b-d) Typical colorimetric readouts of the dummy WEs with separation membranes with (b) too small, (c) proper, and (d) too large sizes.*

Table 1. *The E-μPAD plasma separation performance with different sizes of filtration membranes (n = 21 for each membrane diameter).*

Blood membrane diameter (mm)	Blood leakage (%)	Unsuccessful rate (%)	Success rate (%)
10	66.7	9.5	23.8
11	52.4	28.6	19.0
12	19.0	0	81.0
13	4.8	0	95.2
14	0	85.7	14.3

Calibration of the E-μPAD using artificial blood plasma samples. The E-μPAD was calibrated using artificial blood plasma (ABP) samples spiked with the three cardiac protein markers, cTnI, BNP-32, and D-Dimer. The left plasma separation flap was not involved in this calibration experiments. The ABP sample served as a practical surrogate for the whole blood testing [56], and its detailed preparation protocol is described in Supplementary Information Note 2 [57]. The three markers were spiked in the ABP at 10-fold dilutions to cover the major measurement ranges of the commercial cardiac POC tests [58]. 3 μL of the spiked ABP sample was directly added to each WE and incubated at room temperature for 20 minutes. We then washed each WE with 8 μL of washing buffer and used the right buffer absorption flap to blot the WE. Finally, the electron mediator solution was added to each assembled electrochemical cell for EIS measurement. The measured representative Nyquist plots for detection of the three markers are presented in Figs. 5a-5c. The corresponding calibration curve for each cardiac protein marker was generated by fitting the measured R_{et} value versus the marker concentration into an S-curve through the Hill equation

[34,59], as shown in Figs. 5d-5f (n = 5 for each marker). The LODs were determined to be 4.6 pg/mL (190 fM), 1.2 pg/mL (40 fM), and 146 pg/mL (730 fM) for cTnI, BNP-32, and D-Dimer, respectively, following the LOD definition of the concentration corresponding to three times of the signal standard deviation at zero concentration. The LOD values are below the clinical limits of the specific biomarkers. For cTnI, the normal concentration is 0.04 ng/ml while the heart attack becomes potential above 0.4 ng/ml [60]. For BNP-32, the BNP level less than 100 pg/ml is considered unlikely and alternative causes are considered. The BNP level between 100 and 500 pg/ml indicates the clinical judgement should be used to diagnose heart failure. With BNP level above 500 pg/ml, heart failure or cardiac dysfunction is possible and rapid surgery is suggested [61]. For D-Dimer, the most frequent used medical decision limit is 500 ng/ml [62]. Thus, the developed origami E-μPAD and the EIS assay are able to differentiate between the healthy and non-healthy CVD biomarker concentrations. The achieved LODs of the origami E-μPAD for the cardiac biomarkers are comparable to those of the corresponding standard ELISA kits and the commercial POC products (Supplementary Table S1) [58]. The repeatability of the E-μPAD for the three cardiac markers can be further improved through systematic optimization of the ZnO-NW synthesis process and the EIS detection parameters.

The analytical specificity of the E-μPAD was also examined to confirm the potential sensing interference between the three cardiac protein markers in ABP samples. Three types of spiked ABP samples were prepared: i) spiked with only the target marker, ii) with both the target marker and another cardiac marker (as the sole interference protein), and iii) with both the target marker and the other two cardiac markers (as inference proteins), and the EIS readout signals were compared. To amplify the interference effect, concentrations of the interference markers were set 1,000 times higher than that of the target marker (1 μg/mL vs 1 ng/mL) in the ABP samples. Fig.

S2 presents the specificity testing results for the three cardiac markers, where the notations “A”, “B”, and “C” represent cTnI, BNP-32, and D-Dimer, respectively. Results showed that the presence of the high-concentration interference markers did not significantly alter the EIS signal output compared to the samples with only the target protein, confirming the good analytical specificity of the E-µPAD.

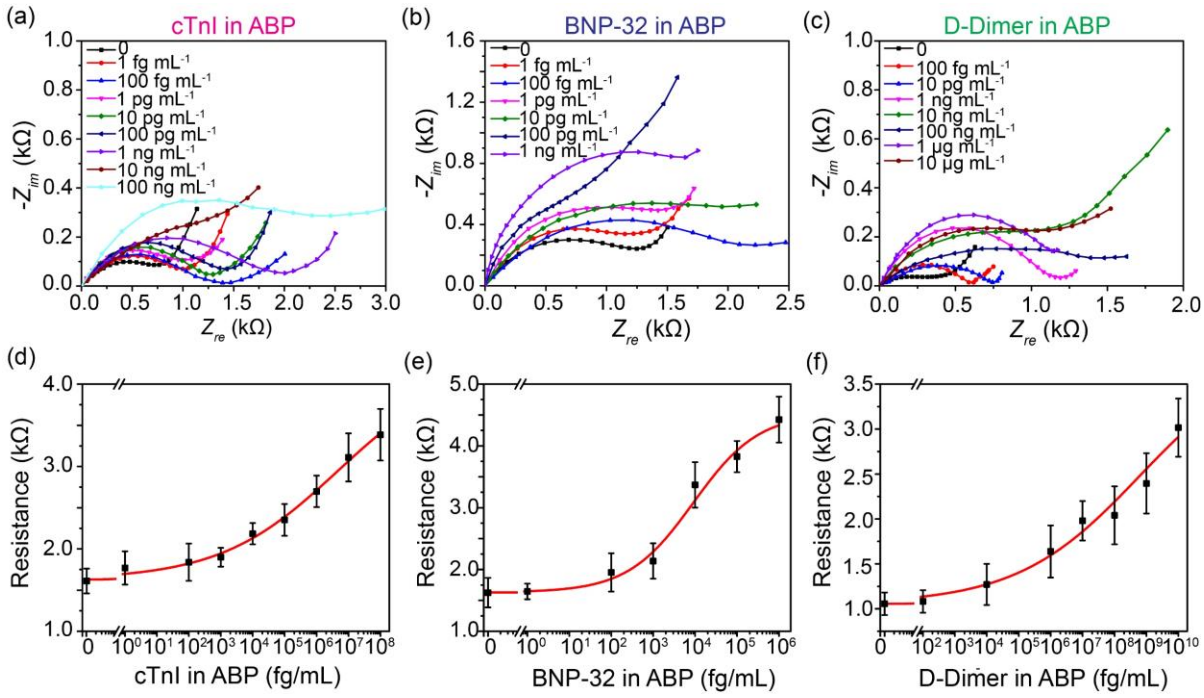

Figure 5. *Calibration results of the E-µPAD using spiked artificial blood plasma (ABP) samples. (a-c) The representative Nyquist plots and (d-f) the corresponding calibration curves (n = 5) measured from the E-µPADs using ABP samples spiked with cTnI, BNP-32, and D-Dimer, respectively.*

Testing of spiked human blood samples. To demonstrate the practical use of the E-µPAD for CVD diagnosis, human blood samples (BioreclamationIVT, LLC, cat: HUMANWBK2-0000409) spiked with the three cardiac protein markers were tested. The original concentrations of the three markers in the commercial human blood sample were firstly quantified using the commercial ELISA kits from Abcam (cat. #ab200016 for human cTnI, cat. #ab193694 for human

BNP-32, and cat. #ab196269 for human D-Dimer). The ELISA testing results indicated that the commercial human blood sample included 90 pg/mL cTnI, 6 pg/mL BNP-32, and 91 ng/mL D-Dimer, as shown in Fig. S3. All values are within the healthy concentration levels. The measured concentrations were the lowest ones of the markers for the spiked human blood samples. The concentration ranges of the three markers in the spiked blood samples were 90 pg/mL–90 ng/mL for cTnI, 6 pg/mL–6 ng/mL for BNP-32, and 91 ng/mL–91 μg/mL for D-Dimer, which covered the typical clinical measurement ranges for the three cardiac markers in human blood: 10-100 ng/mL for cTnI, 8-20 pg/mL for BNP-32, and 350-500 ng/mL for D-Dimer [3,7,58]. In the experiments, 20 μL of spiked human blood samples were added to the plasma separation inlet of an E-μPAD for 20-minute incubation, and the assay was conducted following the steps illustrated in Fig. 2. Fig. 6 shows the generated calibration curves of the E-μPAD for spiked human blood samples, all showing a linear relationship between the readout signal and the marker concentration. The 4-concentration tests still presented a nearly linear behaviour under the log scale of the concentrations. From Figs. 5d–5f, one can see that the calibration curves of the E-μPAD on ABP samples reveal similar linear ranges: 10 pg/mL-100 ng/mL for cTnI, 1 pg/mL-1 ng/mL for BNP-32, and 1 ng/mL-10 μg/mL for D-Dimer. These results confirm that the E-μPAD provides proper linear measurement ranges covering the clinical ones for the three cardiac markers. Note that our calibration curves for artificial plasma (Fig. 5d-f) and whole blood samples (Fig. 6) bear relatively large error bars. The baseline drift issue is critical for EIS sensors and a conditioning step has been reported to help stabilize the R_{ct} baseline prior to receptor functionalization and analyte attachment [63]. However, it can be lengthy and different from one electrode to the other. Thus, the method is hard to be transferred for POC applications. During the experiments, the device fabrication and test protocol has been followed to minimize the manual operation errors. Prospective research can

be done on investigating the baseline drift issue can help further improve the performance. To make our E-µPAD practical for point-of-care diagnosis, we need to improve its biosensing reproducibility by further optimizing the assay protocol and developing a custom-made electrical clipboard for consistent electrical connection with the device. Based on the testing results on spiked ABP and human blood samples, the proposed all-in-one origami E-µPAD holds great potential for POC diagnosis of CVDs.

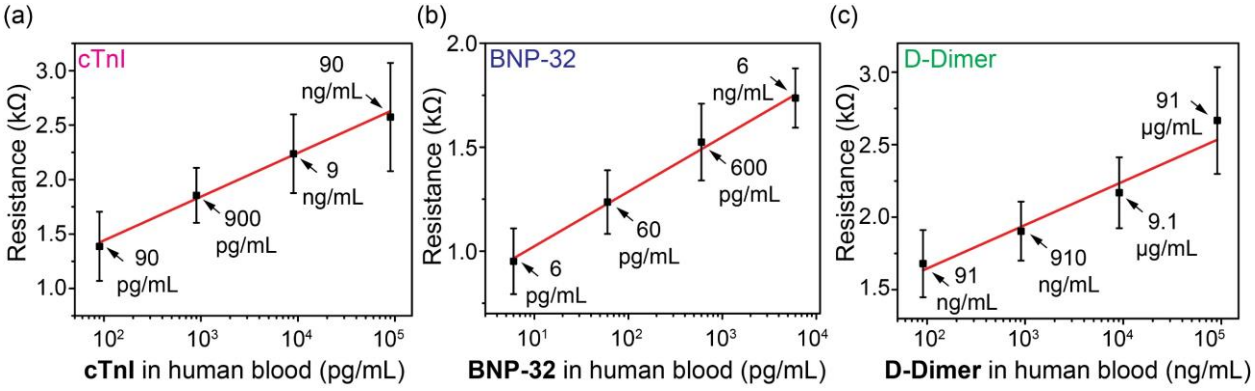

Figure 6. *The EIS calibration curves for detecting CVD biomarkers of (a) cTnI, (b) BNP-32, and (c) D-Dimer in the spiked human whole blood samples with the developed all-in-one origami E-µPADs (n = 5).*

CONCLUSION

To address the urgent need for rapid and reliable CVD protein biomarker diagnosis, we developed an all-in-one origami E-µPAD for multiplexed detection of three typical cardiac protein markers (cTnI, BNP-32, and D-Dimer). The all-in-one origami design of the E-µPAD allowed for on-chip integration of all required components for an EIS-based immunoassay and enabled a rapid and easy assay procedure. The ZnO-NW-coated WE of the E-µPAD improved the device's electrochemical performance thanks to the WE's high surface-area-to-volume ratio and efficient electron-transferring capability. The E-µPAD can detect the three cardiac protein markers in parallel within 46 minutes and perform on-chip plasma separation from a whole blood sample.

This novel paper-based diagnostic technology meets the requirement of a short turnaround time (<60 minutes) for CVD diagnosis. Our calibration results of the E-μPAD on spiked ABP samples showed low LODs of 4.6 pg/mL (190 fM), 1.2 pg/mL (40 fM), and 146 pg/mL (730 fM) for cTnI, BNP-32, and D-Dimer, respectively. These values are comparable to those of the corresponding commercial ELISA kits. The testing of spiked whole blood samples further confirmed the feasibility of the E-μPAD for practical use. It is believed that the reported E-μPAD can be further developed into a practical POC diagnostic tool for rapid and sensitive CVD testing and will also provide a useful diagnostic solution for many other diseases with effective protein markers in the blood.

ACKNOWLEDGEMENT

This work was supported by the Natural Sciences and Engineering Research Council of Canada (grant number: RGPIN-06374-2017), the Canada Foundation for Innovation (grant number: JELF-38428), and the University of Toronto TRANSFORM HF Seed Grant. Z. Q. was supported by the University of Toronto PRiME Fellowship, and H. F. was supported by the McGill Engineering Doctoral Award. P. Song also acknowledges the support from 2020 Natural Science Foundation of the Jiangsu Higher Education (20KJB460024), and Xi'an Jiaotong - Liverpool University via Key Programme Special Fund (KSF-E-39) and Research Development Fund (RDF-18-02-20).

AUTHOR CONTRIBUTIONS

H. F. and Z. Q. designed and performed the experiments, analyzed the data, prepared the presentation items, and wrote the manuscript. X. Li designed and performed the experiments. Y. P. analyzed the data. H. X. fabricated the E-μPADs. P. P., P. S. performed the experiments. X. Liu proposed the idea, designed the experiments, analyzed the data, and revised the manuscript.

REFERENCE

(1) World Health Organization. *Cardiovascular diseases (CVDs)*. World Health Organization. https://www.who.int/news-room/fact-sheets/detail/cardiovascular-diseases-(cvds) (accessed 2022-02-23).

(2) Patibandla, S.; Gupta, K.; Alsayouri, K. *Cardiac Enzymes*; StatPearls Publishing, 2021.

(3) Apple, F. S.; Jesse, R. L.; Newby, L. K.; Wu, A. H. B.; Christenson, R. H. National Academy of Clinical Biochemistry and IFCC Committee for Standardization of Markers of Cardiac Damage Laboratory Medicine Practice Guidelines: Analytical Issues for Biochemical Markers of Acute Coronary Syndromes. *Circulation*. Lippincott Williams & Wilkins April 3, 2007. https://doi.org/10.1161/CIRCULATIONAHA.107.182881.

(4) Ouyang, M.; Tu, D.; Tong, L.; Sarwar, M.; Bhimaraj, A.; Li, C.; Coté, G. L.; Di Carlo, D. A Review of Biosensor Technologies for Blood Biomarkers toward Monitoring Cardiovascular Diseases at the Point-of-Care. *Biosens Bioelectron* **2021**, *171*, 112621. https://doi.org/10.1016/J.BIOS.2020.112621.

(5) Qin, Z.; Peng, R.; Baravik, I. K.; Liu, X. Fighting COVID-19: Integrated Micro- and Nanosystems for Viral Infection Diagnostics. *Matter* **2020**, *0* (0), 1–24. https://doi.org/10.1016/j.matt.2020.06.015.

(6) Ma, Q.; Ma, H.; Xu, F.; Wang, X.; Sun, W. Microfluidics in Cardiovascular Disease Research: State of the Art and Future Outlook. *Microsystems & Nanoengineering 2021 7:1* **2021**, *7* (1), 1–19. https://doi.org/10.1038/s41378-021-00245-2.

(7) Mohammed, M. I.; Desmulliez, M. P. Y. Lab-on-a-Chip Based Immunosensor Principles and Technologies for the Detection of Cardiac Biomarkers: A Review. *Lab on a Chip*. Royal Society of Chemistry February 21, 2011, pp 569–595. https://doi.org/10.1039/c0lc00204f.

(8) Wu, J.; Dong, M.; Santos, S.; Rigatto, C.; Liu, Y.; Lin, F. Lab-on-a-Chip Platforms for Detection of Cardiovascular Disease and Cancer Biomarkers. *Sensors* **2017**, *17* (12), 2934. https://doi.org/10.3390/s17122934.

(9) Du, X.; Su, X.; Zhang, W.; Yi, S.; Zhang, G.; Jiang, S.; Li, H.; Li, S.; Xia, F. Progress, Opportunities, and Challenges of Troponin Analysis in the Early Diagnosis of Cardiovascular Diseases. *Anal Chem* **2022**, *94* (1), 442–463. https://doi.org/10.1021/ACS.ANALCHEM.1C04476.

(10) Das, J.; Gomis, S.; Chen, J. B.; Yousefi, H.; Ahmed, S.; Mahmud, A.; Zhou, W.; Sargent, E. H.; Kelley, S. O. Reagentless Biomolecular Analysis Using a Molecular Pendulum. *Nat Chem* **2021**, *13* (5), 428–434. https://doi.org/10.1038/s41557-021-00644-y.

(11) Spain, E.; Carrara, S.; Adamson, K.; Ma, H.; O'kennedy, R.; De Cola, L.; Forster, R. J. Cardiac Troponin I: Ultrasensitive Detection Using Faradaic Electrochemical Impedance. **2018**. https://doi.org/10.1021/acsomega.8b01758.

(12) Negahdary, M.; Behjati-Ardakani, M.; Sattarahmady, N.; Yadegari, H.; Heli, H. Electrochemical Aptasensing of Human Cardiac Troponin I Based on an Array of Gold Nanodumbbells-Applied to Early Detection of Myocardial Infarction. *Sens Actuators B Chem* **2017**, *252*, 62–71. https://doi.org/10.1016/j.snb.2017.05.149.

(13) Li, F.; Yu, Y.; Cui, H.; Yang, D.; Bian, Z. Label-Free Electrochemiluminescence Immunosensor for Cardiac Troponin I Using Luminol Functionalized Gold Nanoparticles as a Sensing Platform. *Analyst* **2013**, *138* (6), 1844. https://doi.org/10.1039/c3an36805j.

(14) Han, G.-R.; Kim, M.-G. Highly Sensitive Chemiluminescence-Based Lateral Flow Immunoassay for Cardiac Troponin I Detection in Human Serum. *Sensors* **2020**, *20* (9), 2593. https://doi.org/10.3390/s20092593.

(15) Khan, S.; Hasan, A.; Attar, F.; Sharifi, M.; Siddique, R.; Mraiche, F.; Falahati, M. Gold Nanoparticle-Based Platforms for Diagnosis and Treatment of Myocardial Infarction. *ACS Biomaterials Science and Engineering*. American Chemical Society December 14, 2020, pp 6460–6477. https://doi.org/10.1021/acsbiomaterials.0c00955.

(16) Yang, X.; Zhao, Y.; Sun, L.; Qi, H.; Gao, Q.; Zhang, C. Electrogenerated Chemiluminescence Biosensor Array for the Detection of Multiple AMI Biomarkers. *Sens Actuators B Chem* **2018**, *257*, 60–67. https://doi.org/10.1016/j.snb.2017.10.108.

(17) Tang, M.; Zhou, Z.; Shangguan, L.; Zhao, F.; Liu, S. Electrochemiluminescent Detection of Cardiac Troponin I by Using Soybean Peroxidase Labeled-Antibody as Signal Amplifier. *Talanta* **2018**, *180*, 47–53. https://doi.org/10.1016/j.talanta.2017.12.015.

(18) Wang, S.; Li, C.; Saqib, M.; Qi, G.; Ge, C.; Li, H.; Jin, Y. Quasi-Photonic Crystal Light-Scattering Signal Amplification of SiO2-Nanomembrane for Ultrasensitive Electrochemiluminescence Detection of Cardiac Troponin i. *Anal Chem* **2020**, *92* (1), 845–852. https://doi.org/10.1021/acs.analchem.9b03472.

(19) Lin, Y.; Zhang, Y.; Liu, Y.; Cui, K.; Kang, J.; Zhou, Z.; Zhou Zhou, C. How to Choose a Point-of-Care Testing for Troponin. *J Clin Lab Anal* **2020**, *34*. https://doi.org/10.1002/jcla.23263.

(20) Abbott. *i-STAT cTnI Cartridge | Abbott Point of Care*. https://www.globalpointofcare.abbott/en/product-details/apoc/istat-ctnI.html (accessed 2022-02-23).

(21) Quidel. *Quidel Triage MeterPro | Quidel*. https://www.quidel.com/immunoassays/triage-test-kits/triage-meterpro (accessed 2022-02-23).

(22) Martinez, A. W.; Phillips, S. T.; Butte, M. J.; Whitesides, G. M. Patterned Paper as a Platform for Inexpensive, Low-Volume, Portable Bioassays. *Angewandte Chemie - International Edition* **2007**, *46* (8), 1318–1320. https://doi.org/10.1002/anie.200603817.

(23) Ying, B.; Park, S.; Chen, L.; Dong, X.; Young, E. W. K.; Liu, X. NanoPADs and NanoFACEs: An Optically Transparent Nanopaper-Based Device for Biomedical Applications. *Lab Chip* **2020**, *20* (18), 3322–3333. https://doi.org/10.1039/d0lc00226g.

(24) Fu, H.; Song, P.; Wu, Q.; Zhao, C.; Pan, P.; Li, X.; Li-Jessen, N. Y. K.; Liu, X. A Paper-Based Microfluidic Platform with Shape-Memory-Polymer-Actuated Fluid Valves for Automated Multi-Step Immunoassays. *Microsyst Nanoeng* **2019**, *5* (1). https://doi.org/10.1038/s41378-019-0091-0.

(25) Arduini, F.; Cinti, S.; Caratelli, V.; Amendola, L.; Palleschi, G.; Moscone, D. Origami Multiple Paper-Based Electrochemical Biosensors for Pesticide Detection. *Biosens Bioelectron* **2019**, *126*, 346–354. https://doi.org/10.1016/J.BIOS.2018.10.014.

(26) Sun, S.; Wang, Y.; Ming, T.; Luo, J.; Xing, Y.; Liu, J.; Xiong, Y.; Ma, Y.; Yan, S.; Yang, Y.; Cai, X. An Origami Paper-Based Nanoformulated Immunosensor Detects Picograms of VEGF-C per Milliliter of Blood. *Communications Biology 2021 4:1* **2021**, *4* (1), 1–9. https://doi.org/10.1038/s42003-020-01607-8.

(27) Colozza, N.; Caratelli, V.; Moscone, D.; Arduini, F. Origami Paper-Based Electrochemical (Bio)Sensors: State of the Art and Perspective. *Biosensors 2021, Vol. 11, Page 328* **2021**, *11* (9), 328. https://doi.org/10.3390/BIOS11090328.

(28) Dungchai, W.; Chailapakul, O.; Henry, C. S. Electrochemical Detection for Paper-Based Microfluidics. *Anal Chem* **2009**, *81* (14), 5821–5826. https://doi.org/10.1021/ac9007573.

(29) Gutiérrez-capitán, M.; Baldi, A.; Fernández-sánchez, C. Electrochemical Paper-Based Biosensor Devices for Rapid Detection of Biomarkers. *Sensors (Basel)* **2020**, *20* (4). https://doi.org/10.3390/S20040967.

(30) Lee, D.; Bhardwaj, J.; Jang, J. Paper-Based Electrochemical Immunosensor for Label-Free Detection of Multiple Avian Influenza Virus Antigens Using Flexible Screen-Printed Carbon Nanotube-Polydimethylsiloxane Electrodes. *Scientific Reports 2022 12:1* **2022**, *12* (1), 1–11. https://doi.org/10.1038/s41598-022-06101-1.

(31) Peña-Bahamonde, J.; Nguyen, H. N.; Fanourakis, S. K.; Rodrigues, D. F. Recent Advances in Graphene-Based Biosensor Technology with Applications in Life Sciences. *Journal of Nanobiotechnology 2018 16:1* **2018**, *16* (1), 1–17. https://doi.org/10.1186/S12951-018-0400-Z.

(32) Torul, H.; Yarali, E.; Eksin, E.; Ganguly, A.; Benson, J.; Tamer, U.; Papakonstantinou, P.; Erdem, A. Paper-Based Electrochemical Biosensors for Voltammetric Detection of Mirna Biomarkers Using Reduced Graphene Oxide or Mos2 Nanosheets Decorated with Gold Nanoparticle Electrodes. *Biosensors (Basel)* **2021**, *11* (7), 236. https://doi.org/10.3390/BIOS11070236/S1.

(33) Li, X.; Zhao, C.; Liu, X. A Paper-Based Microfluidic Biosensor Integrating Zinc Oxide Nanowires for Electrochemical Glucose Detection. *Microsyst Nanoeng* **2015**, *1* (1), 1. https://doi.org/10.1038/micronano.2015.14.

(34) Li, X.; Liu, X. A Microfluidic Paper-Based Origami Nanobiosensor for Label-Free, Ultrasensitive Immunoassays. *Adv Healthc Mater* **2016**, *5* (11), 1326–1335. https://doi.org/10.1002/adhm.201501038.

(35) Li, X.; Wang, Y. H.; Zhao, C.; Liu, X. Paper-Based Piezoelectric Touch Pads with Hydrothermally Grown Zinc Oxide Nanowires. *ACS Appl Mater Interfaces* **2014**, *6* (24), 22004–22012. https://doi.org/10.1021/am504903b.

(36) Li, X.; Qin, Z.; Fu, H.; Li, T.; Peng, R.; Li, Z.; Rini, J. M.; Liu, X. Enhancing the Performance of Paper-Based Electrochemical Impedance Spectroscopy Nanobiosensors: An Experimental Approach. *Biosens Bioelectron* **2021**, *177* (April 2020), 112672. https://doi.org/10.1016/j.bios.2020.112672.

(37) Boonkaew, S.; Jang, I.; Noviana, E.; Siangproh, W.; Chailapakul, O.; Henry, C. S. Electrochemical Paper-Based Analytical Device for Multiplexed, Point-of-Care Detection of Cardiovascular Disease Biomarkers. *Sens Actuators B Chem* **2021**, *330* (September 2020), 129336. https://doi.org/10.1016/j.snb.2020.129336.

(38) Vasantham, S.; Alhans, R.; Singhal, C.; Nagabooshanam, S.; Nissar, S.; Basu, T.; Ray, S. C.; Wadhwa, S.; Narang, J.; Mathur, A. Paper Based Point of Care Immunosensor for the Impedimetric Detection of Cardiac Troponin I Biomarker. *Biomed Microdevices* **2020**, *22* (1), 1–9. https://doi.org/10.1007/S10544-019-0463-0/TABLES/1.

(39) Wang, L.; Han, Y.; Wang, H.; Han, Y.; Liu, J.; Lu, G.; Yu, H. A MXene-Functionalized Paper-Based Electrochemical Immunosensor for Label-Free Detection of Cardiac Troponin I. *Journal of Semiconductors* **2021**, *42* (9), 092601. https://doi.org/10.1088/1674-4926/42/9/092601.

(40) Mondal, D.; Paul, D.; Mukherji, S. Impedance Spectroscopy-Based Detection of Cardiac Biomarkers on Polyaniline Coated Filter Paper. *IEEE Sens J* **2017**, *17* (16), 5021–5029. https://doi.org/10.1109/JSEN.2017.2717701.

(41) Daniels, J. S.; Pourmand, N. Label-Free Impedance Biosensors: Opportunities and Challenges. *Electroanalysis*. NIH Public Access June 2007, pp 1239–1257. https://doi.org/10.1002/elan.200603855.

(42) Magar, H. S.; Hassan, R. Y. A.; Mulchandani, A. Electrochemical Impedance Spectroscopy (EIS): Principles, Construction, and Biosensing Applications. *Sensors* **2021**, *21* (19), 6578. https://doi.org/10.3390/s21196578.

(43) Li, W.; Li, M.; Ge, S.; Yan, M.; Huang, J.; Yu, J. Battery-Triggered Ultrasensitive Electrochemiluminescence Detection on Microfluidic Paper-Based Immunodevice Based on Dual-Signal Amplification Strategy. *Anal Chim Acta* **2013**, *767* (1), 66–74. https://doi.org/10.1016/j.aca.2012.12.053.

(44) Babuin, L.; Jaffe, A. S. Troponin: The Biomarker of Choice for the Detection of Cardiac Injury. *CMAJ : Canadian Medical Association Journal* **2005**, *173* (10), 1191. https://doi.org/10.1503/CMAJ.050141.

(45) Rasmi, Y.; Mosa, O. F.; Alipour, S.; Heidari, N.; Javanmard, F.; Golchin, A.; Gholizadeh-Ghaleh Aziz, S. Significance of Cardiac Troponins as an Identification Tool in COVID-19 Patients Using Biosensors: An Update. *Front Mol Biosci* **2022**, *9*, 72. https://doi.org/10.3389/fmolb.2022.821155.

(46) Kuwahara, K.; Nakagawa, Y.; Nishikimi, T. Cutting Edge of Brain Natriuretic Peptide (BNP) Research ― The Diversity of BNP Immunoreactivity and Its Clinical Relevance ―. *Circulation Journal* **2018**, *82* (10), CJ-18-0824. https://doi.org/10.1253/CIRCJ.CJ-18-0824.

(47) Reihani, H.; Shamloo, A. S.; Keshmiri, A. Diagnostic Value of D-Dimer in Acute Myocardial Infarction Among Patients With Suspected Acute Coronary Syndrome. *Original Article Cardiol Res* **2018**, *9* (1), 17–21. https://doi.org/10.14740/cr620w.

(48) Zhang, Y. L.; Huang, Y.; Jiang, J. H.; Shen, G. L.; Yu, R. Q. Electrochemical Aptasensor Based on Proximity-Dependent Surface Hybridization Assay for Single-Step, Reusable, Sensitive Protein Detection. *J Am Chem Soc* **2007**, *129* (50), 15448–15449. https://doi.org/10.1021/ja0773047.

(49) Katz, E.; Willner, I. Probing Biomolecular Interactions at Conductive and Semiconductive Surfaces by Impedance Spectroscopy: Routes to Impedimetric Immunosensors, DNA-Sensors, and Enzyme Biosensors. *Electroanalysis*. John Wiley & Sons, Ltd July 1, 2003, pp 913–947. https://doi.org/10.1002/elan.200390114.

(50) Bănică, F.-G. *Chemical Sensors and Biosensors*; John Wiley & Sons, Ltd: Chichester, UK, 2012. https://doi.org/10.1002/9781118354162.

(51) Zhao, Z.; Lei, W.; Zhang, X.; Wang, B.; Jiang, H. ZnO-Based Amperometric Enzyme Biosensors. *Sensors* **2010**, *10* (2), 1216–1231. https://doi.org/10.3390/s100201216.

(52) Pall Corporation. *Separating Plasma from Whole Blood | Pall Corporation*. https://www.pall.com/en/medical/oem-manufacturing/diagnostics-membranes-materials/plasma-separation.html (accessed 2022-02-27).

(53) Caratelli, V.; Ciampaglia, A.; Guiducci, J.; Sancesario, G.; Moscone, D.; Arduini, F. Precision Medicine in Alzheimer's Disease: An Origami Paper-Based Electrochemical Device for Cholinesterase Inhibitors. *Biosens Bioelectron* **2020**, *165*, 112411. https://doi.org/10.1016/J.BIOS.2020.112411.

(54) Batule, B. S.; Seok, Y.; Kim, M. G. Paper-Based Nucleic Acid Testing System for Simple and Early Diagnosis of Mosquito-Borne RNA Viruses from Human Serum. *Biosens Bioelectron* **2020**, *151*. https://doi.org/10.1016/j.bios.2019.111998.

(55) Zhang, H.; Qiu, X.; Zou, Y.; Ye, Y.; Qi, C.; Zou, L.; Yang, X.; Yang, K.; Zhu, Y.; Yang, Y.; Zhou, Y.; Luo, Y. A Dye-Assisted Paper-Based Point-of-Care Assay for Fast and Reliable Blood Grouping. *Sci Transl Med* **2017**, *9* (381). https://doi.org/10.1126/scitranslmed.aaf9209.

(56) Vella, S. J.; Beattie, P.; Cademartiri, R.; Laromaine, A.; Martinez, A. W.; Phillips, S. T.; Mirica, K. A.; Whitesides, G. M. Measuring Markers of Liver Function Using a Micropatterned Paper Device Designed for Blood from a Fingerstick. *Anal Chem* **2012**, *84* (6), 2883–2891. https://doi.org/10.1021/ac203434x.

(57) Liu, L.; Qiu, C. L.; Chen, Q.; Zhang, S. M. Corrosion Behavior of Zr-Based Bulk Metallic Glasses in Different Artificial Body Fluids. *J Alloys Compd* **2006**, *425* (1–2), 268–273. https://doi.org/10.1016/j.jallcom.2006.01.048.

(58) McDonnell, B.; Hearty, S.; Leonard, P.; O'Kennedy, R. Cardiac Biomarkers and the Case for Point-of-Care Testing. *Clinical Biochemistry*. Elsevier May 1, 2009, pp 549–561. https://doi.org/10.1016/j.clinbiochem.2009.01.019.

(59) Cheng, C. M.; Martinez, A. W.; Gong, J.; Mace, C. R.; Phillips, S. T.; Carrilho, E.; Mirka, K. A.; Whitesides, G. M. Paper-Based Elisa. *Angewandte Chemie - International Edition* **2010**, *49* (28), 4771–4774. https://doi.org/10.1002/anie.201001005.

(60) Babuin, L. Troponin: The Biomarker of Choice for the Detection of Cardiac Injury. *Can Med Assoc J* **2005**, *173* (10), 1191–1202. https://doi.org/10.1503/cmaj/051291.

(61) Cao; Jia; Zhu. BNP and NT-ProBNP as Diagnostic Biomarkers for Cardiac Dysfunction in Both Clinical and Forensic Medicine. *Int J Mol Sci* **2019**, *20* (8), 1820. https://doi.org/10.3390/ijms20081820.

(62) Giannitsis, E.; Mair, J.; Christersson, C.; Siegbahn, A.; Huber, K.; Jaffe, A. S.; Peacock, W. F.; Plebani, M.; Thygesen, K.; Möckel, M.; Mueller, C.; Lindahl, B. How to Use D-Dimer in Acute Cardiovascular Care. *Eur Heart J Acute Cardiovasc Care* **2017**, *6* (1), 69–80. https://doi.org/10.1177/2048872615610870.

(63) Gezahagne, H. F.; Brightbill, E. L.; Jin, D. S.; Krishnathas, S.; Brown, B.; Mooney, M. H.; O'Riordan, A.; Creedon, N.; Robinson, C.; Vogel, E. M. Suppression of Impedimetric Baseline Drift for Stable Biosensing. *ECS Sensors Plus* **2022**, *1* (3), 031605. https://doi.org/10.1149/2754-2726/ac8fa1.

For TOC only:

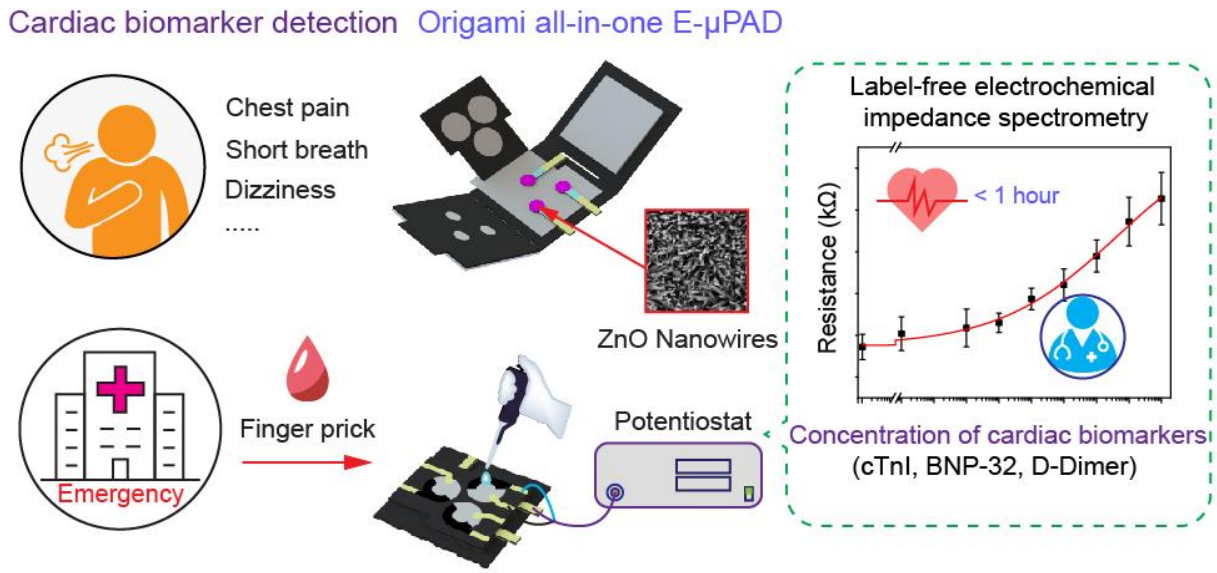
Cardiac biomarker detection
Origami all-in-one E-μPAD
Chest pain
Short breath
Dizziness
.....
Emergency
Finger prick
ZnO Nanowires
Potentiostat
Label-free electrochemical impedance spectrometry
Resistance (kΩ)
< 1 hour
Concentration of cardiac biomarkers
(cTnI, BNP-32, D-Dimer)